

# Development of a Lithium Beam Probe and Measurement of Density Pedestal in JT-60U

Atsushi KOJIMA, Kensaku KAMIYA, Takaaki FUJITA, Hirotaka KUBO, Harukazu IGUCHI<sup>1</sup>, Naoyuki OYAMA, Takahiro SUZUKI, Yutaka KAMADA and the JT-60 Team

*Japan Atomic Energy Agency, Naka, Ibaraki 311-0193, Japan*

<sup>1</sup>*National Institution of Fusion Science, Toki, Gifu 509-5292, Japan*

(Received 16 July 2009 / Accepted 16 March 2010)

A lithium beam probe (LiBP) has been developed for the measurement of electron density profiles with highly spatial and temporal resolutions in JT-60U. Using an electron beam heating ion source with a capability of 10 mA extraction, a 5.5 mA beam has been injected to the plasmas. It corresponds to the equivalent neutral beam current of 2 mA. A spectrum width of the beam emission has been small enough to separate Zeeman splitting. By use of the LiBP, time evolutions of pedestal density profiles during type I and grassy edge localized modes (ELMs) have been obtained for the first time. After a type I ELM crash, the drop of the line-integrated density measured by an interferometer delays by 2 ms later than that of the pedestal density. Comparing the line-integrated density to the line integration of the edge density profile measured by the LiBP, it is found that the recovery from the type I ELM crash is correlated with the reduction of core plasma density. As for grassy ELMs, grassy ELMs have smaller density crashes than that of type I ELMs, which is mainly derived from the narrower ELM affected area.

© 2010 The Japan Society of Plasma Science and Nuclear Fusion Research

Keywords: JT-60U, tokamak, H mode, type I ELM, grassy ELM, edge density, LiBP (lithium beam probe)

DOI: 10.1585/pfr.5.015

## 1. Introduction

ELMy H-mode plasmas are characterized by a pedestal structure and various edge localized modes (ELMs) in the edge region. The H mode operation with ELMs gives us a good confinement and a controllable impurity ejection simultaneously; hence ELMy H-mode plasmas can keep steady-state high performance plasmas. However, a large ELM heat load can damage the divertor plate in future tokamaks such as ITER, which is one of the critical problems. Therefore, ELM physics has been studied to mitigate the ELM heat load [1–6]. In JT-60U, ELM studies for type I ELMs [7–9] and grassy ELMs [10, 11] have been extensively performed. In such ELMy H-mode plasmas, the pedestal structure is formed in a narrow region (4–5 cm) just inside the separatrix. The ELMs collapse the pedestal structure with frequency up to 1 kHz. Therefore, ELM studies require the edge diagnostics having the highly spatial and temporal resolutions, simultaneously. In large devices such as JT-60U, it is difficult for the edge diagnostics to satisfy both the highly spatial and temporal resolutions. In JT-60U, the YAG Thomson scattering systems has been used to measure the time evolution of the density profiles in the whole region of plasmas. However, the spatial channels of the edge region and the repetition rate are not enough for the H-mode and ELM studies. Toward such requests, a lithium beam probe (LiBP) is one of powerful

tools for the edge diagnostics. LiBPs are widely utilized in a lot of tokamak devices, such as DIII-D [12], JET [13] and ASDEX Upgrade [14]. Then, the edge plasma measurement by the LiBP was planned in JT-60U by use of a low energy and a large current Li injector. After the development of the Li injector, the LiBP system with the spatial resolution of 1 cm and the temporal evolution of 0.5 ms has been developed in order to measure the time evolution of the edge density profile during ELMs and the edge current profile. Using the LiBP, the dynamics of the density pedestal has been measured in H-mode plasmas and compared between type I and grassy ELMs. In this paper, the newly-developed LiBP system is introduced and the evolutions of the electron density profiles during ELMs are presented.

## 2. LiBP System on JT-60U

The LiBP system consists of the Li beam injector and detectors as shown in Fig. 1. An active beam diagnostics on large plasma devices are characterized by a long beam line, which is 6.5 m from the neutralizer in the JT-60U LiBP. To achieve the high quality of the beam emission signal even with the long beam line, the Li ion gun having a capability of a high-brightness with a low-divergence angle was developed [15]. As for the injector, the ion gun has been installed in the diagnostic platform and injects a 10 keV Li<sup>0</sup> beam to the plasmas vertically. In a

author's e-mail: kojima.atsushi@jaea.go.jp

case of the beam injection, a leakage magnetic field of  $3 \times 10^{-2}$  T generated by poloidal field coils seriously affects steering of the  $\text{Li}^+$  beam toward a neutralizer, since the leakage magnetic field of  $10^{-4}$  T is the marginal value to control the 10 keV  $\text{Li}^+$  beam within the long and narrow beam line. Therefore, the ion gun has been shielded by a magnetic shield which has a capability to reduce magnetic field strength from  $3 \times 10^{-2}$  T to  $2 \times 10^{-5}$  T. The magnetic shield has a three-layer structure and consists of SS400 (40 mm) and Permalloy (2 mm dual layer). Since the magnetic shield has worked successfully, the beam displacement due to the magnetic field is negligible during the beam injection even with the magnetic field. As for the detectors, an optical system has been installed at a horizontal port of JT-60U, having the oblique line of sight to the beam axis to separate the Doppler shifted beam emission from the thermal Li emission. It consists of an optical lens, photo elastic modulators (PEMs), a linear polarizer and an optical fiber array. The optical lens has the magnification of 0.2 and the effective diameter of 120 mm. S-TIH6 material is utilized for the lens which is the alternative to the low Verdet constant glass SFL6 [16]. In front of the lens, a slit is installed to reduce solid angle to the direction of the beam axis. The optical fiber array has 20 channels for the diagnostics and  $3 \times 2$  channels for the beam profile and beam axis monitors. The spatial resolution for the plasma radius is 1 cm, depending on the inter-

section of the beam, the line of sight and the flux surface of plasmas. Four fibers with each core diameter of 1 mm are bundled in each diagnostic channel. The 600  $\mu\text{m}$  fibers are arranged at up- and down-stream for the beam profile monitors, each of which has 3 channels perpendicular to the beam axis. Through the optical fibers with length of 21 m, photo-multipliers with an etalon ( $\Delta\lambda \sim 0.1$  nm) and bandpass filters ( $\Delta\lambda \sim 1$  nm) detects the Doppler-shifted Li beam emission ( $\lambda = 670.78$  nm) of the 2s-2p resonance line. The high-speed oscilloscopes have been utilized for the data-acquisition system in the LiBP [17].

### 3. Operation of LiBP

During the experimental campaign, an operation period of the LiBP has been determined by an overhaul cycle mainly caused by a short life time of the neutralizer. The neutralizer with Na of 1 g can keep the neutralization efficiency for 10 hours at temperature of 300 degree Celsius. Typically, Na of 8 g is reserved in the Na reservoir tank. Then, the neutralizer needs to be refilled after 10 operation days. The optimization of the neutralizer configuration or the alternative methods of the charge exchange are issues to improve an availability of the LiBP diagnostics. A life time of the ion source with  $\beta$  eucryptite of 1.5 g is estimated to be 52.5 Asec. In a case of a 5 mA ion beam extraction, which is the typical value, the ion source can keep the beam extraction for 10000 s corresponding to 200-300 shots which is longer life time than that of the neutralizer.

The ion gun of the LiBP was equipped with the electron beam heating ion source.  $\text{Li}^+$  beam current is maintained by a PID control of the electron beam (EB) power to the ion source as shown in Fig. 2. After high voltages for  $\text{Li}^+$  beam and EB are applied, the EB heating starts to increase the temperature of the ion source shot by shot. After the pre-heating of the ion source, the EB power is decreased to maintain the expected beam current and kept to stabilize the temperature profile of the ion source. Because it takes several 10 seconds for the temperature profile to reach steady state, the ion source needs to be ready before the beam injection to the plasmas. At the beginning of

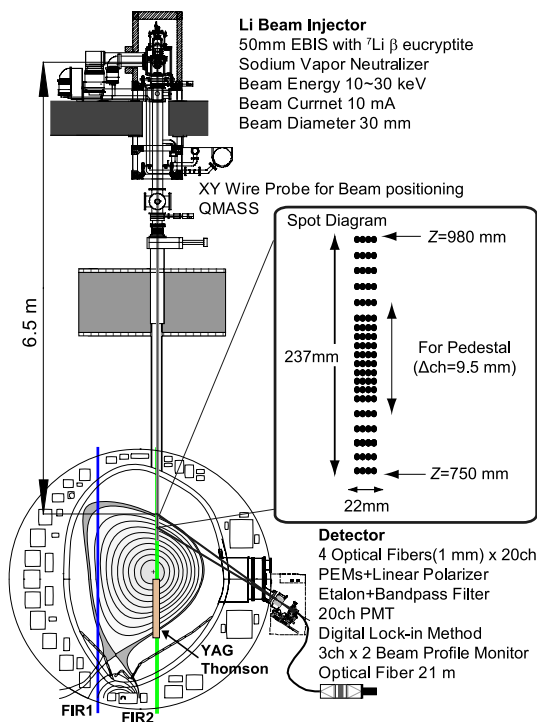


Fig. 1 Schematic view of the lithium beam probe system on JT-60U and expanded view of a spot diagram of the optical system. Arrangement of the diagnostics (YAG Thomson scattering, FIR interferometers) is also shown.

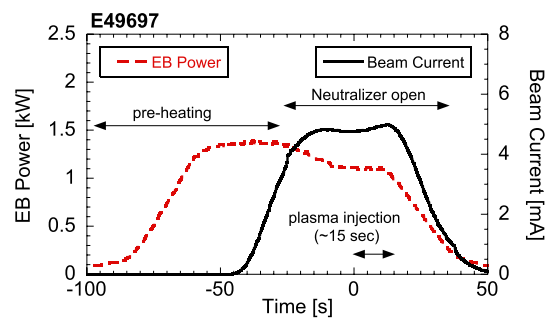


Fig. 2 Operational sequence of the lithium beam probe. High voltages for the acceleration, the Einzel lens and the XY deflectors are applied before the electron beam heating.

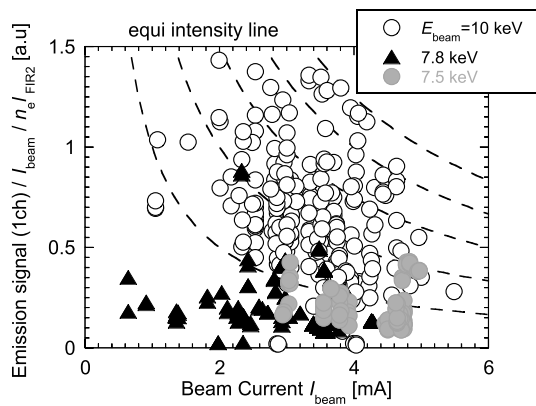


Fig. 3 The dependence of the beam quality on beam energy. Li (1ch) denotes the Li beam emission signal of the most upper channel just inside of the separatrix.

the plasma injection, the relative sensitivity normalization across the all detectors is carried out by use of a gas injection phase for the plasma production in every shot. During the beam injection, beam chopping by changing a pair of high voltages to Y deflectors into a rectangle waveform is used to monitor the unexpected background light. Since the temperature of the ion source is kept about 1500 degree Celsius, the temperature of the anode (without cooling) rises up to 400 degree Celsius, which is equipped with the ion source. A duty cycle of the beam injections is limited by the temperature increase of an insulator, which supports this anode. Typical duty cycle of ON/OFF is 1 min/30 min operations due to cooling of the anode.

For the beam axis alignment, the two pairs of high voltages to the XY deflectors are scanned by high-speed HV amps. And then the Einzel lens voltage is adjusted. The beam position and profile are examined by the XY wire probes in the beam line (without plasma injection) and the beam profile monitors (with plasma injection). The beam alignment is important for the active beam diagnostic because the beam emission intensity strongly depends on the beam quality corresponding to the beam alignment and focusing as shown in Fig. 3. This figure shows the dependence of the beam emission intensity normalized by beam current and the line-integrated electron density along the beam axis. The vertical axis implies the beam intensity which depends on the beam quality such as the beam position control and divergence.

The 10 keV beam injections for the density measurement have been carried out mainly which is the design value of beam energy, and also the 7.5 and 7.8 keV beam injections have been tried to measure the edge current profile; these beam energies depend on the characteristic of the etalon filters. The control of the low energy and large current beams with the long beam line is difficult and requires the accurate alignment and the good controllability. In terms of the beam performance, the higher beam energy is better, however, modest energy of 10 keV beam is ap-

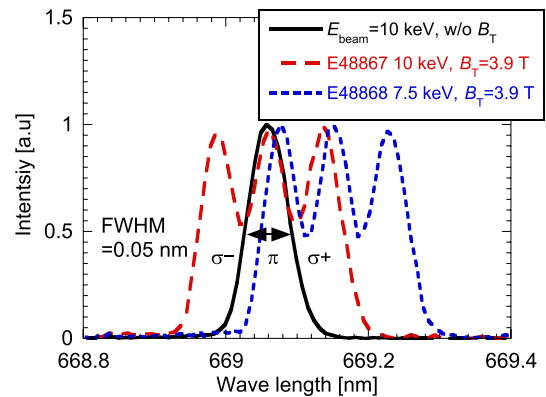


Fig. 4 Doppler-shifted beam emission spectra in the cases of the gas injection at 10 keV beam, OH plasmas at 10 keV and 7.5 keV beams with toroidal field of 3.9 T. The spectrometer CLP-400 was used.

propriate for the pedestal density measurement with its optimum penetration length. To investigate the beam quality, the Doppler-shifted beam emission spectra have been obtained by the injection to gas filled torus (without toroidal magnetic field) and an ohmic heated plasma as shown in Fig. 4. The full width at half maximum of 0.05 nm, which is determined by the beam divergence, solid angle of the optical system and the energy spread of the beam, is small enough to separate each Zeeman splitting spectra. This result suggests that the high-quality beam has been obtained even in the magnetic field.

#### 4. Edge Density Measurement by LiBP

The detailed edge density measurements have been carried out in JT-60U H-mode plasmas. The edge density profiles are calculated from the beam emission signal in the LiBP diagnostic. The conventional density reconstruction method assuming the fully-attenuated beam is applied at this time, in which only the 2s-2p emission is considered and the whole shape of the beam emission profile is estimated from the measured profiles [18]. The reconstruction method including the more detailed atomic process will be developed in the future. The typical beam emission profiles and the reconstructed electron density from L-mode to ELMy H-mode through ELM free H-mode are shown in Fig. 5. The plasma parameters are as follows; plasma current  $I_p = 1.6$  MA, the toroidal magnetic field on the plasma axis  $B_T = 3.9$  T, safety factor at 95% flux surface  $q_{95} = 4.3$ , triangularity  $\delta = 0.34$  and co-toroidal rotation case. After the NBI heating has been applied, the edge density and the edge temperature increase gradually until the first ELM. As the edge density increases, the beam emission profiles and the reconstructed area of the electron density become narrower. After the ELM free phase, type I ELMs with frequency of 18 Hz appear from 5.3 sec.

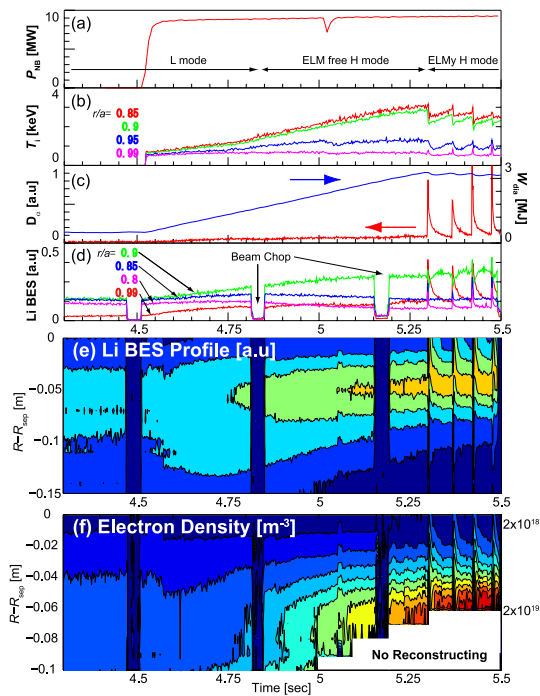


Fig. 5 Edge density profile measurement from L to H mode plasmas. (a) Neutral beam heating power. (b) Ion temperature measured by a charge exchange recombination spectroscopy. (c)  $D\alpha$  emission and stored energy. (d) Profile of Li beam emission signal where  $R_{sep}$  is the separatrix position. The background signal is subtracted by the beam chopping method. (e) Reconstructed electron density profile from the Li beam emission signal as shown in (d). White region denotes the region unable to be reconstructed.

The time evolution of the edge density profiles during the ELM cycle has been observed by the LiBP. Just after an ELM crash, the beam emission increases near the separatrix, suggesting that the electron density near the separatrix increases due to the ELM crash. The background signal is estimated from the beam-off signal in the beam chopping method. In this case, the duty cycle of the beam chopping is ON/OFF = 0.3/0.05 s. The background signal seems to come from the reflection of bremsstrahlung light on the first wall. The typical beam emission and the reconstructed edge density profiles are shown in Fig. 6. In the L-mode plasmas as shown in Fig. 6 (a), the beam emission profile is almost identical to the density profile, and no background signal has been observed. In such low density cases, the density profile is calculated from the beam emission profiles by using a coefficient. The coefficient is obtained from the relation between the beam emission signal and edge density near the separatrix at the timing of high density plasmas in the same shot, whose edge density profile can be calculated by the conventional attenuation method. In the H-mode plasmas as shown in Fig. 6 (b), the beam is fully attenuated within the observation area. This is an optimum condition for the density profile recon-

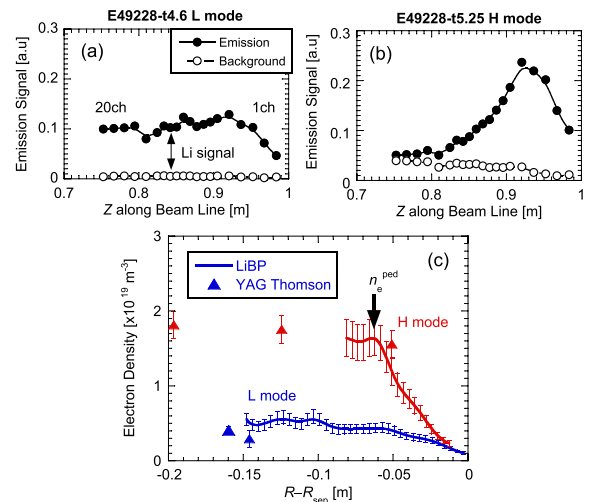


Fig. 6 Typical beam emission and background signal profiles on (a) L mode and (b) H mode plasmas. (c) Comparison of the reconstructed electron density from the profiles of (a) and (b).

struction. The clear pedestal structure has been observed in H-mode plasmas, having the density pedestal width about 5 cm as shown in Fig. 6 (c). The density profile measured by the LiBP is consistent with that measured by the YAG Thomson scattering system. The penetration length of the 10 keV beam is short enough to reconstruct the edge density profile of the JT-60U H-mode plasmas. Moreover, a slower velocity of the 10 keV beams than other LiBPs gives the good spatial resolution of 1 cm which depends on a life time of the radiative transition from 2p state (26.9 ns).

## 5. Density Profile during ELMs

The time evolution of one cycle of type I ELMs is investigated in ELMy H-mode plasmas with co-toroidal rotations. The arrangement of the diagnostics for electron density measurement is shown in Fig. 1. The edge density profile measured by the LiBP covers around 8 cm from the separatrix along with the same vertical line as a FIR interferometer (FIR2) and the YAG Thomson scattering. Using these diagnostics, the line-integrated densities can be compared. However, as for a density collapse due to ELMs, it is noted that the initiation of the ELM collapse has the poloidal asymmetry, and occurs in the localized region near the midplane at a low field side with a time scale of 100-350  $\mu$ s [19]. Such a non-uniform density collapse in a flux surface relaxes with a time scale of several 100  $\mu$ s (determined by the connection length and the ion sound speed). Since the temporal resolution of the LiBP is 0.5 ms, which is not fast enough to observe the asymmetry collapse, the observed drop of pedestal density due to the ELM crash in this paper represents the results after a propagation and relaxation of the initial collapse.

Figure 7 (a) shows the evolution of one cycle of the

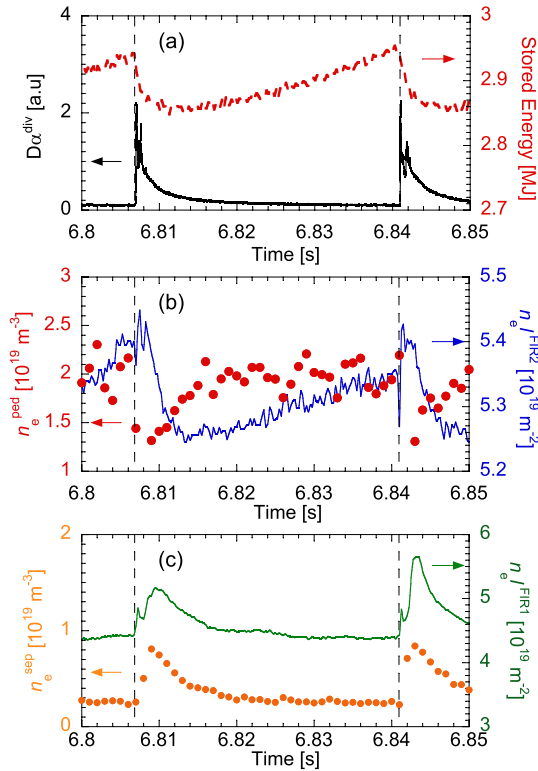


Fig. 7 One cycle of the type I ELMs. (a)  $D\alpha$  emission and stored energy. (b) Pedestal electron density measured by the LiBP and line-integrated electron density measured by FIR2. (c) Electron density near the separatrix measured by the LiBP and line-integrated electron density measured by FIR1. The chords of the interferometers are shown in Fig. 1.

type I ELMs. The ELM energy loss is 89 kJ corresponding to  $\Delta W_{\text{ELM}}/W_{\text{ped}}$  of 8%, which is relatively large in JT-60U ELMy H-mode plasmas. Frequency of ELMs,  $f_{\text{ELM}}$ , is 37 Hz. Figure 7 (b) shows the comparison of the evolution of electron density at the pedestal top  $n_e^{\text{ped}}$  and line-integrated electron density  $n_e l^{\text{FIR2}}$ , where  $n_e^{\text{ped}}$  is measured by the LiBP and  $n_e l^{\text{FIR2}}$  is measured by the FIR interferometer along the same chord as the beam line of the LiBP. Figure 7 (c) also shows the comparison of electron density near the separatrix  $n_e^{\text{sep}}$  measured by the LiBP and line-integrated electron density  $n_e l^{\text{FIR1}}$ , where  $n_e l^{\text{FIR1}}$  is measured by the FIR interferometer along the vertical line on a high field side. Using the LiBP, the evolution of the density pedestal has been observed. A drop of the pedestal density  $n_e^{\text{ped}}$  reaches  $\sim 30\%$  due to an ELM crash. Just after the ELM crash ( $t = 6.807\text{--}6.814$  s), the increase of the separatrix density  $n_e^{\text{sep}}$  implies the increase of electron density in the scrape-off layer (SOL). These phenomena indicate that the pedestal structure of electron density is collapsed due to the ELM crash. After the pedestal structure is collapsed, the density pedestal recovers in 10 ms and almost become steady state. On the other hand, line-integrated electron density  $n_e l^{\text{FIR2}}$  decreases later than the timing of the drop

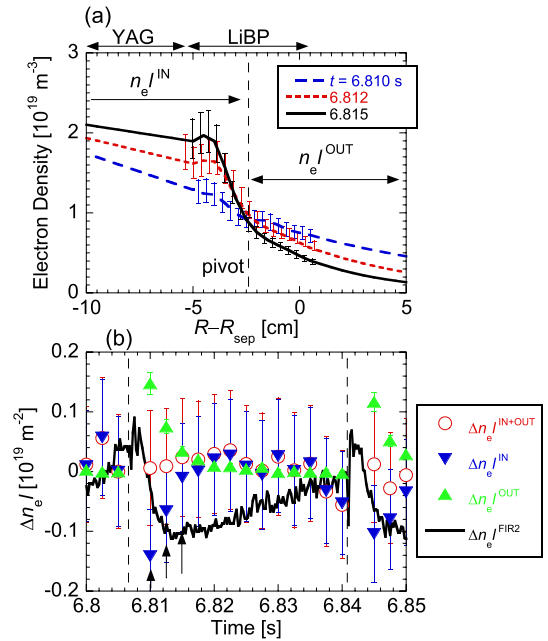


Fig. 8 (a) Evolution of the radial profile of the density pedestal during one cycle of type I ELM. (b) Comparison of the line-integrated electron densities estimated by the LiBP and the FIR interferometer.

of  $n_e^{\text{ped}}$ . As shown in Fig. 7 (b), the time scale of the recovery of the pedestal density is close to the reduction of  $n_e l^{\text{FIR2}}$ . As for the electron density around the separatrix, a waveform of  $n_e^{\text{sep}}$  is similar to that of  $n_e l^{\text{FIR1}}$ . These results suggest that the reduction of  $n_e l^{\text{FIR2}}$  may be correlated with the recovery of  $n_e^{\text{ped}}$ , while the behavior of  $n_e l^{\text{FIR1}}$  is caused by the increase of electron density around the separatrix. It is noted that increase of  $n_e l^{\text{FIR1}}$  and  $n_e^{\text{sep}}$  may not suggest the density exhaust; a time scale of the density collapse due to ELMs is about 200  $\mu\text{s}$  [20]. Increase of these densities results from the increase of the SOL density caused by the enhanced recycling effect due to ELM crashes [20].

Figure 8 (a) shows the evolution of the edge density profile measured with the LiBP and the YAG Thomson scattering. A pivot of the electron density profile is located at 3 cm inside from the separatrix. Inside of the pivot, electron density increases as well as the recovery of  $n_e^{\text{ped}}$ , while, outside of the pivot, electron density decreases as well as the reduction of  $n_e^{\text{sep}}$ . In order to compare line-integrated electron density to  $n_e l^{\text{FIR2}}$ , electron density in the pedestal region is line-integrated such as  $n_e l^{\text{IN}}$  and  $n_e l^{\text{OUT}}$  along the beam line of the LiBP where the boundary condition of the integration is the pivot position. The boundary condition is also determined by the ELM affected area which is assumed to be 15 cm estimated by the YAG Thomson scattering data. The time evolutions of  $n_e l^{\text{IN}}$  and  $n_e l^{\text{OUT}}$  are compared to  $n_e l^{\text{FIR2}}$  as shown in Fig. 8 (b).  $\Delta n_e l$  in the vertical axis indicates the variations of these line-integrated electron densities from the pre-ELM value. In this case,  $\Delta n_e l^{\text{IN}}$  and  $\Delta n_e l^{\text{OUT}}$  are almost

balanced ( $\Delta n_e I^{IN} + \Delta n_e I^{OUT} \sim 0$ ) during this cycle. However,  $\Delta n_e I^{FIR2}$  decreases 2 ms after the ELM collapse. Furthermore,  $\Delta n_e I^{IN}$  is comparable to  $\Delta n_e I^{FIR2}$ . From these results, the slow reduction of  $n_e I^{FIR2}$  implies a redistribution of electron density to compensate most of the lost pedestal density because  $\Delta n_e I^{FIR2} - (\Delta n_e I^{IN} + \Delta n_e I^{OUT})$  denotes the change of electron density in the core region;  $\Delta n_e I^{FIR2}$  of  $0.1 \times 10^{19} \text{ m}^{-2}$  corresponds to 2% reduction of electron density in the core region. If the decrease of  $n_e I^{OUT}$  compensates the increase of  $n_e I^{IN}$ ,  $\Delta n_e I^{FIR2}$  needs to be zero.

## 6. Density Profile during Grassy ELM

Grassy ELMs are characterized by the narrow ELM affected area of density and temperature pedestals, thus the drop of the stored energy is smaller than that of type I ELMs [12,21]. The density pedestal during grassy ELMs has been investigated by the LiBP as shown in Fig. 9. The plasma parameters are as follows;  $I_p = 1.0 \text{ MA}$ ,  $B_T = 4.0 \text{ T}$ ,  $q_{95} = 4.3$ ,  $\delta = 0.54$ ,  $f_{ELM} = 200 \text{ Hz}$ ,  $P_{NB} = 9.4 \text{ MW}$  and the toroidal rotation frequency at the pedestal top  $V_T^{ped} = 0.9 \text{ kHz}$ .  $f_{ELM}$  of 200 Hz at  $V_T^{ped} = 0.9 \text{ kHz}$  is consistent with the previous experiment [10]. The drop of the pedestal density is 20%, which is smaller than that of type I ELM. It is noted that grassy ELMs with large amplitude are shown here while typical grassy ELMs with  $f_{ELM} > 500 \text{ Hz}$  has much smaller crashes which are comparable to a noise level of the LiBP [21]. The evolution of electron density during the grassy ELM measured by the LiBP is shown in Fig. 10(a). In comparison with that of the type I ELM, the grassy ELM has the narrower ELM affected area. The pivot is located at 2 cm inside of the separatrix, which is outside than that of the type I ELM. These results suggest that grassy ELMs occur in the narrow region just inside the separatrix. The line-integration has been performed in same way as the type I ELM case. The change of the line-integrated densities  $\Delta n_e I^{IN}$ ,  $\Delta n_e I^{OUT}$  has been observed as shown in Fig. 10(b). The line-integrated density in the pedestal region  $\Delta n_e I^{IN} + \Delta n_e I^{OUT}$  shows that

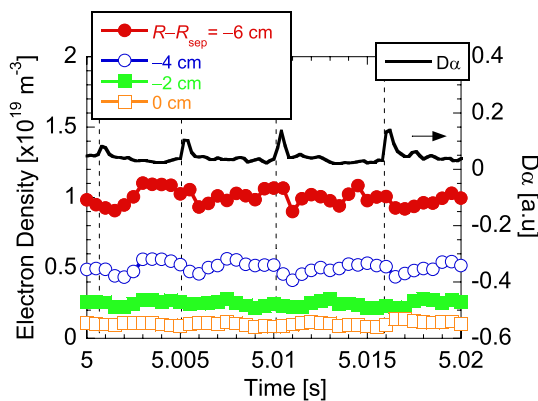


Fig. 9 Edge electron density measure by the LiBP during grassy ELM with frequency of 200 Hz.

$\Delta n_e I^{IN}$  is slightly larger than  $\Delta n_e I^{OUT}$ . However, the drop of  $\Delta n_e I^{IN}$  due to the grassy ELM is much smaller than that of the type I ELM, suggesting the small particle loss of the grassy ELM. The difference in density loss fractions between type I and grassy ELMs at the pedestal top, 30% and 20% respectively, can not explain observed difference of  $\Delta n_e I^{IN}$ , suggesting the radial extension of the ELM affected area is main cause for the difference. The comparison of the line integrated densities is performed; however, the observed change of  $\Delta n_e I^{IN} + \Delta n_e I^{OUT}$  is comparable to the noise level in  $\Delta n_e I^{FIR2}$  and much smaller than the component of core region in  $\Delta n_e I^{FIR2}$ .

## 7. Conclusion

The LiBP system has been developed in JT-60U to measure the edge electron density with highly spatial (1 cm) and temporal (0.5 ms) resolutions. The beam current of 5.5 mA has been injected to the plasmas, corresponding to the equivalent neutral beam current of 2 mA. Moreover, the observed spectrum width is small enough to separate the Zeeman splitting spectra. Therefore, the low energy and large current beams have been achieved in JT-60U LiBP.

Although the electron beam heating ion source has a capability of large beam extraction, the control of the temperature profile of the ion source and the large heat load to other components are still problems in a case of the measurement of the long pulse operation. In the operation of the LiBP, the beam alignment is also one of dif-

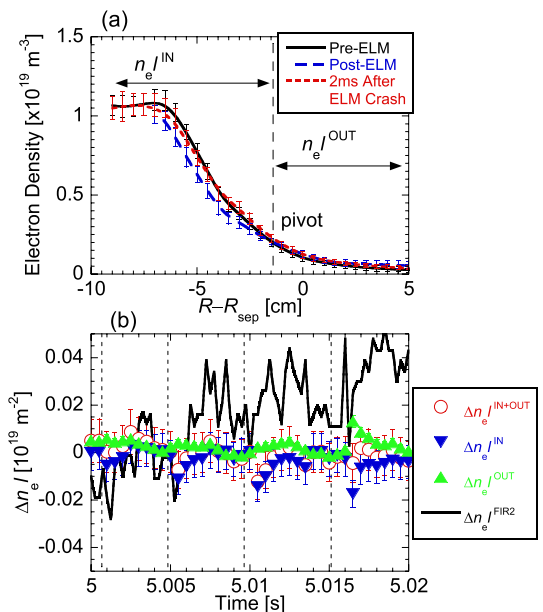


Fig. 10 (a) Evolution of the radial profile of the density pedestal during one cycle of grassy ELM. The profiles are obtained by 0.2 s averaging, corresponding to 40 ELMs. (b) Comparison of the line-integrated electron densities estimated by the LiBP and the FIR interferometer.

facilities and adjusted shot by shot using the beam profile monitors, since the obtained signal strongly depends on the beam quality. The beam alignment method during the injection is required for the long pulse operation. As for the availability of the diagnostic, the life time of the neutralizer or other charge exchange method which is free from an alkali metal vapor needs to be developed.

As the results of the careful beam control, the edge density profiles during type I and grassy ELMs have been obtained for the first time in JT-60U. By comparing the edge density profile to the line-integrated density, the behavior of electron density in the core plasma after ELM crash has been estimated. As a result, the electron density in core region might compensate for the edge density collapse by type I ELM, because the reduction of the line-integrated density delays from the ELM crash. As for the grassy ELM, because the density reduction is small, the behavior of the line-integrated density is unclear. However, the integrated edge density measured by the LiBP suggested that the recovery processes of type I and grassy ELMs might not be same because the behaviors of balance of the edge density ( $\Delta n_e l^{\text{IN}} + \Delta n_e l^{\text{OUT}}$ ) were different.

It is important to investigate the behavior of the density pedestal for the predictions of the pedestal performance and ELM activity. So far, JT-60U did not have the fast diagnostic for the edge density profile, thus the study of the density pedestal will be progressed by the LiBP results.

## Acknowledgments

This research was partly supported by the Grant-in-

Aid for Young Scientists (B) 19760603, the Grant-in-Aid for Young Scientists (A) 19686056 and the Grant-in-Aid for Scientific Research (S) 17106013 Japan Society for the Promotion of Science.

- [1] H. Zohm, *Plasma Phys. Control. Fusion* **38**, 105 (1996).
- [2] J.W. Connor, *Plasma Phys. Control. Fusion* **40**, 531 (1998).
- [3] W. Suttrop, *Plasma Phys. Control. Fusion* **42**, A1 (2000).
- [4] E.J. Doyle *et al.*, *Progress in the ITER Physics Basis Chapter 2*, *Nucl. Fusion* **47**, S18 (2007).
- [5] N. Oyama, *Journal of Physics: Conference Series* **123**, 012002 (2008).
- [6] T.E. Evans *et al.*, *Phys. Rev. Lett.* **92**, 235003 (2004).
- [7] H. Urano *et al.*, *Phys. Rev. Lett.* **95**, 035003 (2005).
- [8] H. Urano *et al.*, *Nucl. Fusion* **48**, 045008 (2008).
- [9] K. Kamiya *et al.*, *Plasma Fusion Res.* **2**, 005 (2007).
- [10] N. Oyama *et al.*, *Plasma Phys. Control. Fusion* **49**, A249 (2007).
- [11] N. Oyama *et al.*, *Nucl. Fusion* **45**, 871 (2005).
- [12] D.M. Thomas *et al.*, *Rev. Sci. Instrum.* **61**, 3040 (1990).
- [13] Z.A. Pietrzyk *et al.*, *Plasma Phys. Control. Fusion* **35**, 1725 (1993).
- [14] E. Wolfrum *et al.*, *Rev. Sci. Instrum.* **77**, 033507 (2006).
- [15] A. Kojima *et al.*, *Rev. Sci. Instrum.* **79**, 093502 (2008).
- [16] B.W. Rice, *Fusion. Eng. Des.* **34-35**, 135 (1997).
- [17] G. Matsunaga *et al.*, *Fusion. Eng. Des.* **82**, 207 (2007).
- [18] S. Sasaki *et al.*, *Rev. Sci. Instrum.* **64**, 1699 (1993).
- [19] N. Oyama *et al.*, *Nucl. Fusion* **43**, 1250 (2003).
- [20] N. Oyama *et al.*, *Nucl. Fusion* **44**, 582 (2004).
- [21] A. Kojima *et al.*, *Nucl. Fusion* **49**, 115008 (2009).